Accepted Manuscript

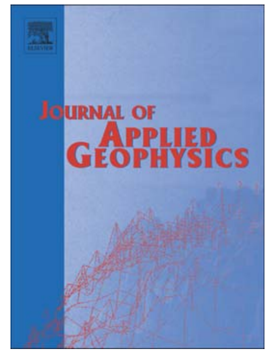

Effects of source and cavity depths on wave-fields in layered media

Hua-You Chai, Siang-Huat Goh, Kok-Kwang Phoon, Chang-Fu Wei, Dian-Ji Zhang

PII: S0926-9851(14)00158-X
DOI: doi: 10.1016/j.jappgeo.2014.05.017
Reference: APPGEO 2511

To appear in: *Journal of Applied Geophysics*

Received date: 10 October 2013
Revised date: 22 May 2014
Accepted date: 23 May 2014

Please cite this article as: Chai, Hua-You, Goh, Siang-Huat, Phoon, Kok-Kwang, Wei, Chang-Fu, Zhang, Dian-Ji, Effects of source and cavity depths on wave-fields in layered media, *Journal of Applied Geophysics* (2014), doi: 10.1016/j.jappgeo.2014.05.017

Effects of source and cavity depths on wave-fields in layered media

Hua-You Chai[a,c]; Siang-Huat Goh[b]; Kok-Kwang Phoon[b]; Chang-Fu Wei[c] ; Dian-Ji Zhang[a]

[a]*School of Resource and Civil Engineering, Wuhan Institute of Technology, Wuhan 430073, China.*

[b]*Department of Civil and Environmental Engineering, National University of Singapore, Singapore 117576, Singapore*.

[c]*State Key Laboratory of Geomechanics and Geotechnical Engineering, Institute of Rock and Soil Mechanics, Chinese Academy of Sciences, Wuhan 430071, China*.

Keywords: Layered half space; Buried source; Rayleigh waves; Leaky Lamb waves; Thin Layer Method; Scattered waves.

Corresponding author:

Dr. Hua-You Chai

School of Resource and Civil Engineering, Wuhan Institute of Technology, Wuhan 430073, China.

E-mail: Chy_RSM@Hotmail.com

Abstract

The multiple modes of Rayleigh waves (R-waves) or leaky Lamb waves (L-waves) may be present in the activated and/or the back-scattered wave-fields. The presence of these waves in the wave-fields is related to the source and the cavity depths. Two types of layered media are used to investigate the influences of the source and the cavity depths. One is the layered half space where the half space is stiffer than all the overlying layers; the other is the pavement system where there is significant velocity contrast between layers and the shear velocity of layers decreases with the layer depth. The discrete displacement expressions developed for spherical point sources are used to study the effects of the source depth on the excitability and the propagation behavior of R-waves or leaky L-waves. In layered half spaces, the multiple modes of R-waves can be activated by the sources within a certain depth. The effective phase velocity of these activated modes is derived. In pavement systems, the leaky L-waves can be activated by the sources at any depth. The discrete displacement expressions of the scattered waves are derived and used to evaluate the effects of the cavity depth on the presence of R-waves or the leaky L-waves in the back-scattered wave-field.

1. Introduction

In horizontally layered half spaces, there are the multiple modes of R-waves covering a wide range of frequency (Foti, 2000; Lu and Zhang, 2004; Strobbia, 2003; Tokimatsu et al., 1992b). When the stiffness of layer increases with layer depth, the first (fundamental) mode of R-waves dominates the surface-wave field over the majority of frequency range. However, when softer layers or stiffer layers are trapped in the shallow soil, the higher modes play an important role in the surface-wave field (Gucunski and Woods, 1992; Tokimatsu et al., 1992b).

R-waves activated by the surface sources dominate the surface wave-field (i.e. full wave field at the surface). The energy of R-waves is confined to a shallow depth. The extent of this depth depends on the frequency of R-waves. It increases with decreasing frequency. An anomalous feature that locates within the depth where R-waves pass through will scatter the R-waves. The surface-wave field will be disturbed by these scattered waves both in time and frequency domains (António and Tadeu, 2001; Boström and Kristensson, 1983; Chai et al., 2012a; Ganji et al., 1997; Gelis et al., 2005; Höllinger and Ziegler, 1979; Tadeu et al., 2002, 2006) and these disturbances can be used to characterize the anomalous feature (Vallamsundar, 2007; Vogelaar, 2001; Grandjean and Leparoux, 2004; Nasseri-Moghaddam et al., 2007; Park et al., 1998, 1999; Xia et al., 2007). Although the detectable depth (depth in which the energy of the R-waves is confined) can be increased by decreasing the dominant frequency of sources, the generation of R-waves at very low frequencies is quite difficult using the active sources. Passive waves, which are induced by microtremors of the earth or vibrations of the background, comprise very low frequency components (<10 Hz) (Morikawa et al., 2004; Nasseri-Moghaddam et al., 2007; Park et al., 2005; Tokimatsu et al., 1992a). However, the detection layout and the analysis methods are not well developed for these passive waves. It is more promising to detect deep anomalous features using the body waves. Since R-waves activated by the surface sources are relatively strong in the surface wave-field, the presence of R-waves may severely mask the reflections of the body waves. Buried sources are often used to strengthen the reflections of the body waves and to suppress R-waves. Because the buried sources are important for detection of deep anomalous features, it is helpful to investigate effects of the buried sources and the anomalous features on the excitability of R-waves and the presence of R-waves in the back-scattered wave-field, respectively.

The surface response of a homogeneous, elastic half space to impulsive internal P-wave and S-wave point sources was investigated by Pinney (1954). The integral displacement equation for R-waves for point sources in simple structural models was presented by Anderson (2011). There is one non-dispersive normal mode of R-waves in homogenous half spaces. However, effects of the buried sources on the excitability of this mode are not easily analyzed from the implicit integral expressions presented by these studies. To simplify the analyses, effects of the source and the cavity depths on the wave-field in homogeneous half spaces are investigated using the discrete method (Chai et al., 2013). In comparison with R-waves in homogenous half spaces, there are multiple modes of R-waves and the leaky L-waves in the layered half spaces and the pavement systems, respectively. These modes are dispersive. The excitability and the propagation behavior of R-waves and the leaky L-waves generated by the surface sources were investigated by Gucunski and Woods (1992), Tokimatsu et al. (1992b) and Ryden and Lowe (2004), respectively. To our best knowledge, comparable work for the buried sources and the anomalous features has not been conducted in layered media. The main contribution of this paper is to apply the thin layer method to analyze the excitability of R-waves or leaky L-waves and the presence of R-waves or leaky L-waves in the back-scattered wave-fields in layered media. Based on these analyses, the wave components in the activated and the back-scattered wave-fields can be effectively analyzed and an appropriate source depth can be found to suppress R-waves.

The objectives of this paper work are as follows: (i) investigate effects of the source depth on the excitability and the propagation behavior of R-waves or leaky L-waves in two types of layered media, and (ii) investigate effects of the cavity depth on the presence of R-waves or the leaky L-waves in the back-scattered wave-field. To achieve the above goals, the displacement expressions of the activated R-waves and the generalized body waves (including the leaky L-waves) are first presented based on the work proposed by Kausel (1999) for the spherical point source. The displacements of these waves are related to the variations of the modal amplitudes with depth. The excitability of R-waves or leaky L-waves is then investigated by analyzing the variations of modal amplitudes with depth. The effective phase velocity of the activated R-waves is derived from the displacement expression of R-waves. When a cavity is present in the layered media, the displacement of the waves scattered from one point is also proposed in the discrete form and divided into two terms corresponding to R-waves and the generalized body waves, respectively. By doing so, the method for the buried sources can be applied to analyze effects of the cavity depth on the presence of R-waves or the leaky L-waves in the back-scattered wave-field. Some numerical results are presented to verify these analyses.

2. Wave-field activated by buried spherical point source

2.1 *Discrete displacement expression*

Consider a horizontally homogeneous, elastic layered medium containing a small spherical cavity of radius a with center located at $(0,0,z_s)$ in the cylindrical coordinates r, θ and z, and a harmonically oscillating pressure with amplitude p acting on the spherical inner surface, as shown in Fig. 1. When $a \to 0$, the vertical discrete displacement can be approximately expressed as (Kausel, 1999)

$$u_z(z,r,z_s,\omega) \approx -\frac{3(\lambda+2\mu)}{4\mu}\,\bar{p}\left[-\frac{1}{4\mathrm{i}}\sum_{l=1}^{2N}\phi_z^l(z)\phi_x^l(z_s)k_l H_0^{(2)}(k_l r)+\frac{1}{4\mathrm{i}}\sum_{l=1}^{2N}\frac{\partial\phi_z^l(z)}{\partial z}\phi_z^l(z_s)H_0^{(2)}(k_l r)\right], \quad (1)$$

where $\bar{p}=\frac{4}{3}\pi a^3 p$ is the source strength; λ and μ are Lamé's constants of the layer containing the spherical source; $\phi_x^l(z)$, $\phi_z^l(z)$ and k_l are the functions of the horizontal and the vertical shapes and the wavenumber of the l-th mode, respectively; $H_0^{(2)}(k_l r)$ is the second kind Hankel functions of the zero order; N is the number of thin layers. There are $2N$ modes. These modes can be classified into two parts: one part corresponds to R-waves; the second part corresponds to the generalized body waves. By rearranging these modes according to the wave types, Eq. (1) can be regrouped as

$$u_z(z,r,z_s,\omega) = -\frac{3(\lambda+2\mu)}{4\mu}\,\bar{p}\left[-\frac{1}{4\mathrm{i}}\sum_{l=1}^{L_\alpha(\omega)}\phi_{z\alpha}^l(z)\phi_{x\alpha}^l(z_s)k_{\alpha l}H_0^{(2)}(k_{\alpha l}r)-\frac{1}{4\mathrm{i}}\sum_{m=1}^{M_R(\omega)}\phi_{zR}^m(z)\phi_{xR}^m(z_s)k_{Rm}H_0^{(2)}(k_{Rm}r)\right.$$

$$\left.+\frac{1}{4\mathrm{i}}\sum_{l=1}^{L_\alpha(\omega)}\frac{\partial\phi_{z\alpha}^l(z)}{\partial z}\phi_{z\alpha}^l(z_s)H_0^{(2)}(k_{\alpha l}r)+\frac{1}{4\mathrm{i}}\sum_{m=1}^{M_R(\omega)}\frac{\partial\phi_{zR}^m(z)}{\partial z}\phi_{zR}^m(z_s)H_0^{(2)}(k_{Rm}r)\right]. \quad (2)$$

The subscripts α and R denote parameters corresponding to the generalized body waves and R-waves, respectively. The sum of the modes for generalized body waves and R-waves is equal to 2N, i.e. $L_\alpha(\omega)+M_R(\omega)=2N$. The number of modes for each wave type, $L_\alpha(\omega)$ or $M_R(\omega)$, is related to the soil profile and frequency. The vertical displacements of R-waves and the generalized body waves u_{zR} and $u_{z\alpha}$ in Eq. (2) can be rewritten as

$$u_{zR}(z,r,z_s,\omega)=-\frac{3(\lambda+2\mu)\mathrm{i}}{16\mu}\,\overline{p}\sum_{m=1}^{M_R(\omega)}\beta_m(z,z_s,\omega)H_0^{(2)}(k_{Rm}r)\,,$$

$$u_{z\alpha}(z,r,z_s,\omega)=-\frac{3(\lambda+2\mu)\mathrm{i}}{16\mu}\,\overline{p}\sum_{l=1}^{L_\alpha(\omega)}\gamma_l(z,z_s,\omega)H_0^{(2)}(k_{\alpha l}r)\,, \qquad (3)$$

where

$$\beta_m(z,z_s,\omega)=\left[\phi_{zR}^m(z)\phi_{xR}^m(z_s)k_{Rm}-\phi_{zR}^m(z)_{,z}\phi_{zR}^m(z_s)\right],$$

$$\gamma_l(z,z_s,\omega)=\left[\phi_{z\alpha}^l(z)\phi_{x\alpha}^l(z_s)k_{\alpha l}-\phi_{z\alpha}^l(z)_{,z}\phi_{z\alpha}^l(z_s)\right]. \qquad (4)$$

2.2 *Propagation behavior of the activated R-waves*

The mode in the natural state (i.e. no source) is often termed as “normal mode” (Kausel, 1999; Ryden and Park, 2004) or “natural mode” (Chai et al., 2012a). The term “activated mode” is here used to denote the mode activated by the sources. The multiple activated modes constructively or destructively interfere with each other. The superposed R-waves travel at so-called “effective” or “apparent” phase velocity (Chai et al, 2011, 2012b; Foti, 2000; Strobbia, 2003; Tokimatsu et al., 1992b). If the material damping can be ignored, the modal amplitudes and wavenumbers of R-waves are real. Under such conditions, the effective phase velocity can be derived following the method used by Chai et al. (2012b) as

$$c_{zR}(r,z,z_s,\omega)=\frac{\omega}{\hat{k}_{zR}(r,z,z_s,\omega)}=\frac{\omega\sum_{m=1}^{M_R}\sum_{\hat{m}=1}^{M_R}\hat{B}_{m\hat{m}}[Y_0(k_{Rm}r)Y_0(k_{R\hat{m}}r)+J_0(k_{Rm}r)J_0(k_{R\hat{m}}r)]}{\sum_{m=1}^{M_R}\sum_{\hat{m}=1}^{M_R}\hat{B}_{m\hat{m}}k_{Rm}[Y_0(k_{Rm}r)J_1(k_{R\hat{m}}r)-J_0(k_{Rm}r)Y_1(k_{R\hat{m}}r)]}, \quad (5)$$

where $\hat{B}_{m\hat{m}}=\beta_m(z,z_s,\omega)\beta_{\hat{m}}(z,z_s,\omega)$; $J_n(k_R r)$ (n=0, 1) and $Y_n(k_R r)$ are the first and the second kind Bessel functions of the nth order.

In the far field where the offset is large relative to the maximum wavelength of R-waves, i.e. $k_R r>>1$, the expression in Eq. (5) can be simplified to

$$c_{zR}(r,z,z_s,\omega)\approx\frac{\omega\sum_{m=1}^{M_R}\sum_{\hat{m}=1}^{M_R}B_{m\hat{m}}\cos[(k_{Rm}-k_{R\hat{m}})r]}{\sum_{m=1}^{M_R}\sum_{\hat{m}=1}^{M_R}B_{m\hat{m}}k_{Rm}\cos[(k_{Rm}-k_{R\hat{m}})r]}=\frac{\sum_{m=1}^{M_R}\sum_{\hat{m}=1}^{M_R}B_{m\hat{m}}\cos[(k_{Rm}-k_{R\hat{m}})r]}{\sum_{m=1}^{M_R}\sum_{\hat{m}=1}^{M_R}B_{m\hat{m}}c_{Rm}^{-1}\cos[(k_{Rm}-k_{R\hat{m}})r]}, \quad (6)$$

where $B_{m\hat{m}}=(k_{Rm}k_{R\hat{m}})^{-1/2}\hat{B}_{m\hat{m}}$, c_{Rm} is the phase velocity of the m-th normal mode.

2.3 *Propagation behavior of the leaky Lamb waves*

There are symmetrical (S) and anti-symmetrical (A) L-waves in free plates. In a plate overlying soft soils, the waves in the plate will radiate into the underlying soils. These waves are not the real L-waves and often called as leaky L-waves (or quasi-Lamb waves). The characteristics of the normal leaky modes, such as the dispersion, the attenuation, the variation of modal amplitude with depth and the excitability, were investigated by Ryden and Lowe (2004), Ryden and Park (2004) and Ryden et al. (2004). For a given pavement, the number and the excitability of the leaky modes are related to the frequency components and the depth of the sources. The number of activated leaky modes increases with frequency. The excitability of the mode increases with the modal amplitude at the source depth. The pavement profile adopted by Ryden and Lowe (2004), as shown in Fig. 1(b) is used to investigate the leaky L-waves. The densities and Poisson's ratios of layers and the half space base are assumed to be 2000 kg/m^3 and 0.35. The zero-phase wavelets of the source can simplify resolution because traces containing zero-phase wavelets will have seismic interfaces located in general at the centers of the peaks and troughs of the trace. Ricker wavelet is one of the zero-phase wavelets, which is widely used in synthetic seismograms (Kallweit and Wood, 1982). The expressions in the time and the frequency domains are as follows:

$$s(t) = (1 - 2\pi^2 f_M^2 t^2) e^{-\pi^2 f_M^2 t^2} , \quad S(f) = \frac{2}{\sqrt{\pi}} \frac{f^2}{f_M^3} e^{-\frac{f^2}{f_M^2}} , \tag{7}$$

where f_M is the peak (or center) frequency. The small radius and the peak frequency of the spherical point source in the following axisymmetrical finite element simulations are assumed to be 0.1 m and 100 Hz, respectively. The spectra contour of the surface responses of the pavement system for the source at depth = 1.5 m is given in Fig. 2. The effective phase velocities of the activated leaky modes can be obtained from the amplitude peaks in the spectra (see the white dashed line). Comparing the effective velocities and the dispersion curve of the first anti-symmetrical mode (A0) of Lamb waves in the first free layer of the pavement, it can be found that the trend of the effective phase velocity is similar to the dispersion of the A0 mode.

3. Effects of source depth in layered media

3.1 *Layered half spaces*

It can be seen from Eq. (3) that the component of the *m*-th activated R-wave mode in the surface wave-field at a given offset *r* is related to the modal parameters $\phi_{zR}^m(0)$, $\phi_{xR}^m(z_s)$, $\phi_{zR}^m(0)_{,z}$ and $\phi_{zR}^m(z_s)$. Thus, Eq. (3) can be used to analyze effects of the source depth z_s on the surface-wave field. The layered half spaces where a softer layer is sandwiched between two stiff layers, as shown in Fig. 1(a), are used to study effects of source depth on the modal excitability of R-waves. The densities and Poisson's ratios of the layers and the half space are assumed to be 1800 kg/m^3 and 0.3 for two different layer thicknesses.

The dispersions and the vertical surface amplitudes of the normal modes over the frequency range of interest (less than 500 Hz) are given in Figs. 3(a) and 3(b) for the case of thinner layers (Case I). The spectrum of the Ricker wavelet source with the peak frequency of 100Hz is also plotted in Fig. 3(a). It can be seen that only the first normal mode exists in the major part of the frequency range of the source. It implies that the higher modes can be ignored in the activated wave-field. The modal shapes $\phi_{xR}(z)$ and $\phi_{zR}(z)$ are related to the soil profile and frequency. The first modal shape at the peak frequency of 100 Hz is given in Fig. 3(c). In the soil with thicker layers (Case II), there are 16 modes within the frequency range of interest. The dispersions and the vertical surface amplitudes of the first four normal modes are presented in Figs. 4(a) and 4(b) to illustrate the behavior of the higher modes. It can be found from Fig. 4(a) that there are multiple modes within the frequency range of the source. These modes may be activated by the source. The vertical shapes $\phi_{zR}^{m}(z)$ ($m = 1, \cdots, 4$) of the first four modes at 100 Hz are given in Fig. 4(c). It can be seen that the modal shapes $\phi_{zR}^{m}(z)$ attenuate exponentially in the half space, but vary erratically within the overlying layers. The similar characteristics can be found for the horizontal shapes $\phi_{xR}^{m}(z)$. Thus, the energy of the activated R-waves will decay and can be ignored if the source depth in the half space is sufficiently deep. When the source is located in the overlying layers, the energy may be strengthened or weakened according to the modal shapes. The depths over which energy concentrates are deeper for the higher normal modes at a given frequency. Thus, the source may be located beyond the depth where energy concentrates for low modes, but within the depths where concentrates for higher modes. In this scenario, the energy of the low modes is weak while energy of the higher modes may be relatively strong in the surface-wave field. When the source is located far beyond the depths where energy concentrates for the normal modes, R-waves can be ignored and the body waves will dominate the surface wave-field. Since the characteristics of modal shapes, such as attenuating exponentially in the half space, varying erratically within the overlying layers and deeper energy concentrating depths for higher modes, are same for all types of layered half spaces, the conclusions drawn also hold for other types of layered half spaces.

In the following, some finite element simulations are presented and the wave components are analyzed using the afore-mentioned method. The wave components activated by buried sources are illustrated in Fig. 5. We first pay attention to the activated wave-field. The wave scattering due to the presence of the cavities will be discussed in Section 4. The contour plot of the surface responses activated by the source at depth = 1.2 m is shown in Fig. 6(a). Since R-waves are confined in shallow depths, the activated R-waves can be easily identified in the snapshot of the particle velocity field given in Fig. 6(b), where the symbol P stands for P-waves radiated from the source; PP_0 and PS_0 denote the dilatational and transverse components of the reflections of the P-waves at the free surface. It can be seen in Fig. 6(a) that R-waves travel in a dispersive way due to the dispersive behavior of the first normal mode. For Case II, the contour plot of the surface responses to the source at depth = 0.8 m is given in Fig. 7(a). The different types of waves are identified in the particle velocity contour presented in Fig. 7(b). The R-waves superposed by the multiple activated modes nearly travel at the effective velocity of 167 m/s, which is approximately equal to the phase velocity of R-waves in the half space with the properties of the first layer (Chai et al., 2012a). Since the activated modes in the surface-wave field are influenced by the source depth, the effective phase velocity of the activated R-waves is not only related to the frequency and soil stiffness profile, but also to the source depth [see Eq. (5)].

3.2 Pavement systems

Since R-waves are only present at very low frequencies in the pavement systems (Jones, 1962), the leaky L-waves play an important role in the surface wave-field over most frequencies. The pavement profile is given in Fig. 1(b). The contour plot of the surface responses is shown in Fig. 8 for the source at depth = 1.5 m. The waves travelling at average phase velocities of 390 m/s and 228 m/s correspond to the leaky L-waves (the dispersion is shown in Fig. 2) and the direct P-waves from the source, respectively. Increasing the source depth, the contour plot of the surface responses and a snapshot of particle velocity field for the source at depth = 6 m are given in Figs. 9(a) and (b), respectively. The leakage of the leaky L-waves into the underlying soils can be identified in Fig. 9(b). The leaky L-waves are still strongly energetic in the surface wave-field shown in Figs. 9(a) and 9(b) for such a deep source. This can be explained from the fact that the modal shapes $\phi^{l}_{x\alpha}(z_s)$ and $\phi^{l}_{z\alpha}(z_s)$ related to the leaky L-waves do not attenuate with depth in the half space base like those of R-waves. The leaky L-waves can be activated by the buried source at any depth.

4. Effect of cavity depth on wave scattering

4.1 *Scattered wave field*

For layered media with anomalies acted by a source at the position vector $\mathbf{x}_s$, the *i*-th (i=1, 2, 3) component of the full displacement $u_i(\mathbf{x},\mathbf{x}_s)$ at the position vector $\mathbf{x}$ can be divided into two parts as (Campman, 2005; Riyanti, 2005)

$$u_i(\mathbf{x},\mathbf{x}_s) = u_i^{inc}(\mathbf{x},\mathbf{x}_s) + u_i^{sc}(\mathbf{x},\mathbf{x}_s) \quad , \tag{8}$$

where $u_i^{inc}(\mathbf{x},\mathbf{x}_s)$ denotes the displacement of the direct wave field generated by the source at the position $\mathbf{x}_s$ in the layered media without any anomaly and $u_i^{sc}(\mathbf{x},\mathbf{x}_s)$ represents the displacement of the scattered wave field in the presence of the anomalies with volume = *D*.

$$u_i^{inc}(\mathbf{x},\mathbf{x}_s) = W(\omega) u_{ik}^{G}(\mathbf{x},\mathbf{x}_s) , \tag{9}$$

where ω is angular frequency; $W(\omega)$ denotes the source function in the frequency domain; $u_{ik}^{G}(\mathbf{x},\mathbf{x}_s)$ is the *i*-th component of Green's functions at the position $\mathbf{x}$ due to a point pulse source directed in the *k*-th direction (*k*=1, 2, 3, corresponding to *x*, *y* and *z* coordinates, respectively) at the position $\mathbf{x}_s$. The displacements of the scattered waves can be simplified as

$$u_i^{sc}(\mathbf{x},\mathbf{x}_s) \approx \int_{\mathbf{x}'\in D} \omega^2 \Delta\rho(\mathbf{x}') u_{ik}^{G}(\mathbf{x},\mathbf{x}') u_k(\mathbf{x}',\mathbf{x}_s) dV , \tag{10}$$

where $\Delta\rho(\mathbf{x}')$ is the density changes due to the presence of anomalies. Using the discrete Green's functions and rearranging the modes according to the wave types, the integrand of Eq. (10) can be rewritten as (Chai et al., 2012a)

$$\tilde{u}_3^{sc}(\mathbf{x},\mathbf{x}',\mathbf{x}_s)=\frac{\mathrm{i}\omega^2\Delta\rho(\mathbf{x}')}{4}\left\{\left[\sum_{l=1}^{L_\alpha(\omega)}\phi_{x\alpha}^{l}(z)\phi_{z\alpha}^{l}(z')H_1^{(2)}(k_{\alpha l}\hat{r})+\sum_{m=1}^{M_R(\omega)}\phi_{xR}^{m}(z)\phi_{zR}^{m}(z')H_1^{(2)}(k_{Rm}\hat{r})\right]\right.$$

$$\left.\left[\cos\hat{\theta}u_1(\mathbf{x}',\mathbf{x}_s)+\sin\hat{\theta}u_2(\mathbf{x}',\mathbf{x}_s)\right]-\left[\sum_{l=1}^{L_\alpha(\omega)}\phi_{z\alpha}^{l}(z)\phi_{z\alpha}^{l}(z')H_0^{(2)}(k_{\alpha l}\hat{r})+\sum_{m=1}^{M_R(\omega)}\phi_{zR}^{m}(z)\phi_{zR}^{m}(z')H_0^{(2)}(k_{Rm}\hat{r})\right]u_3(\mathbf{x}',\mathbf{x}_s)\right\},\tag{11}$$

where $H_1^{(2)}(k_l r)$ is the second kind Hankel functions of the first order; $\hat{r}$ and $\hat{\theta}$ as shown in Fig. 10 are the local cylindrical coordinates. It can be seen from Eq. (11) that the displacement of the R-waves or the leaky L-waves in the scattered wave-field is related to both the vertical and the horizontal modal amplitudes at the scattering position z'. Thus, the effect of the cavity depth on the presence of the R-waves or the leaky L-waves in the back-scattered surface wave-field can be analyzed from Eq. (11).

4.2 *Rectangular cavities in layered half spaces*

The descriptions of a rectangular cavity are given in Fig. 5. As mentioned above, R-waves can be activated by a shallow source. The activated R-waves are scattered at a shallow cavity (Chai et al., 2012a). The scattered R-waves may obscure the scattering of P-waves radiated from the source. A deep source is set at depth of 6 m so that the source is far beyond the depth over which energy concentrates for the first normal mode. Thus, the components of the incident waves $u_i(\mathbf{x}',\mathbf{x}_s)$ (i=1, 2, 3) are mainly the body waves. The presence of R-waves in the back-scattered wave-field due to the direct R-waves can be excluded. For Case I, a shallow rectangular cavity is set at: r_n=15 m, r_f=19 m, h_t= 0.8 m and h_b=1.8 m. The cavity is located within the depth over which energy concentrates for the first normal mode (see Fig. 3), i.e. the modal amplitudes within that depth are relatively large. When the direct waves encounter the cavity, each scattering point at the cavity can be regarded as a new source. R-waves are obviously observed in the back-scattered surface wave-field, as shown in Fig. 11, where P-P and P-S waves denote the dilatational and transverse components of P-waves scattered at the cavity, respectively. This phenomenon is consistent with the prediction from Eq. (11). The same cavity is set in Case II and the source is located at depth = 7 m. A similar phenomenon can be observed in the back-scattered surface wave-field, as shown in Fig. 12. To examine the influence of the deep cavity, two cavities are set at locations where the modal amplitudes are small [see the modal shapes in Figs. 3(c) and 4 (c)]. One cavity is set at locations of r_n=15 m, r_f=19 m, h_t= 4 m, h_b=5 m for Case I; the other is located at r_n=15 m, r_f=19 m, h_t= 7 m, h_b=8 m for Case II. It can be inferred from Eq. (11) that R-waves in the back-scattered wave-field are weak and can be ignored, as shown in Figs. 6 and 7. The above analyses show that the component of R-waves in the back-scattered wave-field is strengthened or weakened when the cavity is located within the depth over which energy concentrates for the normal modes; when the cavity is located far beyond this depth, R-waves in the back-scattered wave-field can be ignored.

4.3 *Rectangular cavities in pavement systems*

Since the modal shapes $\phi^{l}_{x\alpha}(z)$ and $\phi^{l}_{z\alpha}(z)$ corresponding to the leaky L-waves do not attenuate with depth, it is not surprising that the leaky L-waves may be present in the back-scattered wave-field for cavities at any depth [see Eq. (11)]. This can be verified by numerical results. The contour plot of the surface responses is given in Fig. 13 for the shallow cavity at locations of r_n=15 m, r_f=19 m, h_t=1 m and h_b=2 m and the source at depth = 6 m. It can be seen that the back scattered wave-field is dominated by the back leaky L-waves. When a deep cavity is located at r_n=15 m, r_f=19 m, h_t=4 m and h_b=5 m, the leaky L-waves is still obvious in the back-scattered wave-field, as shown in Fig. 9(a).

5. Conclusions

The effects of the source and the cavity depths on the presence of R-waves or the leaky L-waves can be analyzed from variations of the modal amplitudes with depth. The discrete displacement expressions are derived for this purpose.

In the layered half spaces, the number and the excitability of R-wave modes depend on the frequency components and the depth of sources. The activated modes interfere with each other. For a given soil profile, the effective (or apparent) phase velocity of the superposed R-waves is frequency and source depth dependent. Since the modal amplitudes attenuate exponentially with the depth in the half spaces, the activated R-waves will correspondingly decay with the depth of sources located in the half spaces. Thus, from the soil profile and the frequency components of the source, an appropriate depth can be estimated for the buried sources to suppress the activated R-waves.

When a cavity is present in the layered half spaces, the presence of R-waves in the back-scattered wave-field is mainly controlled by the ratio of the cavity depth to the energy concentrating depth of R-waves. The conclusions drawn for the source depth hold for the cavity depth.

In pavement systems, the number and the excitability of the leaky modes are also related to the frequency components and the depth of sources. Since the modal shapes oscillate with depth, some modes of the leaky L-waves with low attenuation can appear in the activated and/or the back-scattered wave-fields for deep sources and/or deep cavities.

Acknowledgements

This work is funded by Defence Science and Technology Agency, Singapore under project agreement No. POD1014347.

References

Anderson, J. 2011. Source effects on surface wavefields. http://www.ees.nmt.edu/outside/Geop/Classes/GEOP523/Docs/JAnderson.pdf.

António, J., Tadeu, A., 2001. 3D scattering by multiple cylindrical cavities buried in an elastic formation. European Journal of Mechanics - A/Solids 20(3), 367-383.

Boström, A., Kristensson, G., 1983. Scattering of a pulsed Rayleigh wave by a spherical cavity in an elastic half space. Wave Motion 5, 137-143.

Campman, X.H., 2005. Imaging and suppressing near-receiver scattered seismic waves. Ph. D Thesis, Delft Institute of Applied Mathematics, Delft University of Technology, The Netherlands.

Chai, H.Y., Cui, Y.J., Wei, C.F., 2012b. A Parametric Study of Effective Phase

Velocity of Surface Waves in Layered Media. Computers and Geotechnics 44, 176-184.

Chai, H.Y., Goh, S.H., Phoon, K.K., Wei, C.F., 2013. Effects of source and cavity depths on wave-fileds in homogeneous half spaces. Journal of Applied Geophysics 93, 52-59.

Chai, H.Y., Phoon, K.K., Goh, S.H., Wei, C.F., 2012a. Some theoretical and numerical observations on scattering of Rayleigh waves in media containing shallow rectangular cavities. Journal of Applied Geophysics 83, 2012, 107-119.

Chai, H.Y., Phoon, K.K., Wei, C.F., Lu, Y.F., 2011. Analysis of effects of active sources on observed phase velocity based on the thin-layer method. Journal of Applied Geophysics 73(1), 49-58.

Foti, S., 2000. Multistation methods for geotechnical characterization using surface waves. Ph.D. thesis, Politecnico di Torino, Italy.

Ganji, V., Gucunski, N., Maher, A., 1997. Detection of underground obstacles by SASW method—Numerical aspects. Journal of Geotechnical and Geoenvironmental Engineering 123(3), 212-219.

Gelis, C., Leparoux, D., Virieux, J., Bitri, A., Operto, S., Grandjean, G., 2005. Numerical modeling of surface waves over shallow cavities. Journal of Environmental and Engineering Geophysics 10 (2), 111–121.

Grandjean, G., Leparoux, D., 2004. The potential of seismic methods for detecting cavities and buried objects: experimentation at a test site. Journal of Applied Geophysics 56 (2), 93– 106.

ACCEPTED MANUSCRIPT

Gucunski, N., Woods, R.D., 1992. Numerical simulation of the SASW test. Soil Dynamics and Earthquake Engineering 11 (4), 213–227.

Höllinger, F., Ziegler, F. 1979. Scattering of pulsed Rayleigh surface waves by a cylindrical cavity. Wave Motion 1, 225-238.

Jones, R., 1962. Surface wave technique for measuring the elastic properties and thickness of pavements: Theoretical development. British Journal of Applied Physics 13, 21-29.

Kallweit, R. S., Wood, L. C., 1982. The limits of resolution of zero-phase wavelets. Geophysics 47(7), 1035-1046.

Kausel, E., 1999. Dynamic point sources in laminated media via the thin-layer method. International Journal of Solids and Structures 36 (31), 4725-4742.

Lu, L.Y., Zhang, B.X., 2004. Analysis of dispersion curves of Rayleigh waves in the frequency — wavenumber domain. Canadian Geotechnical Journal 41(4), 583-598.

Morikawa, H., Sawada, S., Akamatsu, J., 2004. A method to estimate phase velocities of Rayleigh waves using microseisms simultaneously observed at two sites. Bulletin of the Seismological Society of America 94(3), 961-976.

Nasseri-Moghaddam, A., Cascante, G., Phillips, C., Hutchinson, D.J., 2007. Effects of underground cavities on Rayleigh waves—field and numerical experiments. Soil Dynamics and Earthquake Engineering 27 (4), 300–313.

Park, C.B., Miller, R.D., Ryden, N., Xia, J., Ivanov, J., 2005. Combined use of active and passive surface waves. Journal of Environmental and Engineering Geophysics 10(3), 323-334.

Park, C.B., Miller, R. D., Xia, J.H., 1998. Ground roll as a tool to image near-surface anomaly, SEG Expanded Abstract, 874-877.

Park, C.B., Miller, R.D., Xia, J.H., 1999. Detection of near-surface voids using surface waves. SAGEEP 99, Oakland, Calif., 281-286.

Pinney, E., 1954. Surface motion due to a point source in a semi-infinite elastic medium. Bulletin of the Seismological Society of America 44(1), 571-596.

Riyanti, C.D., 2005. Modeling and inversion of scattered surface waves. Ph. D Thesis, Delft Institute of Applied Mathematics, Delft University of Technology, The Netherlands.

Ryden, N., and Lowe, M.J.S, 2004. Guided wave propagation in three-layer pavement structures, Journal of the Acoustical Society of America 116 (5), 2902-2913.

Ryden, N., and Park, C. B., 2004. Surface waves in inversely dispersive media. Near Surface Geophysics 2(4), 187–197.

Ryden, N., Park, C.B., Ulriksen, P., Miller, R.D., 2004. Multimodal Approach to Seismic Pavement Testing. Journal of Geotechnical and Geoenvironmental Engineering 130(6), 636-645.

Strobbia, C., 2003. Surface wave methods —Acquisition, processing and inversion. Ph.D. thesis, Politecnico di Torino, Italy.

Tadeu, A.J.B., António, J.M.P., Kausel, E., 2002. 3D scattering of waves by a cylindrical irregular cavity of infinite length in a homogeneous elastic medium. Computer Methods in Applied Mechanics and Engineering 191 (27-28), 3015-3033.

Tadeu, A.J.B., Mendes, P.A., António, J., 2006. The simulation of 3D elastic scattering produced by thin rigid inclusions using the traction boundary element method. Computers and Structures 84 (31-32), 2242-2253.

Tokimatsu, K., Shinzawa, K., Kuwayama, K.S., 1992a. Use of short period microtremors for Vs profiling. Journal of Geotechnical Engineering 118 (10), 1544–1558.

Tokimatsu, K., Tamura, S., Kojima, H., 1992b. Effects of multiple modes on Rayleigh wave dispersion characteristic. Journal of Geotechnical Engineering 118 (10), 1529–1543.

Vallamsundar, S., 2007. Numerical evaluation of classification techniques for flaw detection. Masters Thesis. University of Waterloo, Waterloo, Ontario, Canada.

Vogelaar, B.B.S.A., 2001. Cavity detection—a feasibility study towards the application of seismic surface wave stack methods for the identification and localization of underground voids. Master These, OYO Center of Applied Geosciences, Archimedesbaan 16, Nieuwegein & University of Utrecht, Department of Earth Sciences, Budapestlaan 4, Utrecht, The Netherlands.

Xia, J.H., Nyquist, J.E., Xu, Y.X., Roth, M.J.S., Miller, R.D., 2007. Feasibility of detecting near-surface feature with Rayleigh-wave diffraction. Journal of Applied Geophysics 62 (3), 244–253.

Stokoe, II. K. H, Joh, S. H., Woods, R. D., 2004. Some contributions of in situ geophysical measurements to solving geotechnical engineering problems. International Conference on Site Characterization (ISC-2), Porto, Portugal, September

19-22, 15-50.

LIST OF FIGURES

plot of the surface responses; and (b) snapshot of particle velocity field.

Fig. 10. Global and local coordinate systems (S: scattering point; P: observation point).

Fig. 11. Contour plot of the surface responses of Case I for the source at depth of 6 m and the rectangular cavity at r_n=15 m, r_f=19 m, h_t= 0.8 m and h_b=1.8 m.

Fig. 12. Contour plot of the surface responses of Case II for the source at depth of 7 m and the rectangular cavity at r_n=15 m, r_f=19 m, h_t= 0.8 m and h_b=1.8 m.

Fig. 13. Contour plot of the surface responses of the pavement system for the source at depth of 6 m and the rectangular cavity at r_n=15 m, r_f=19 m, h_t= 1 m and h_b=2 m.

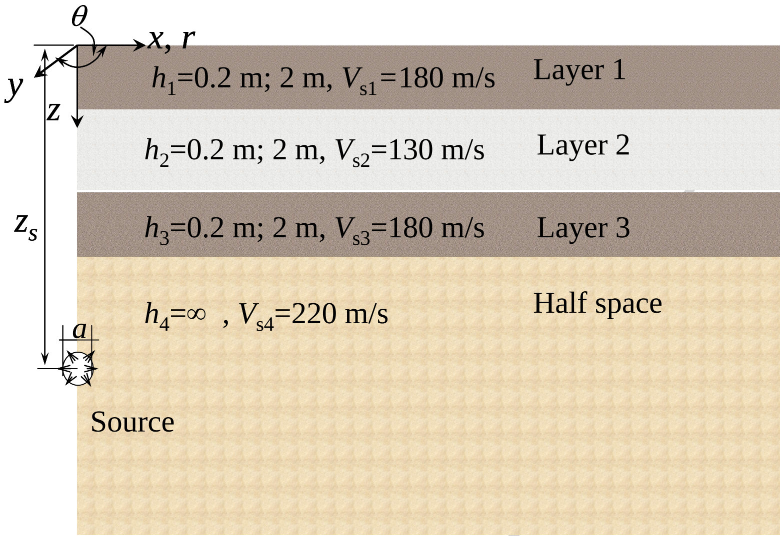

(a)

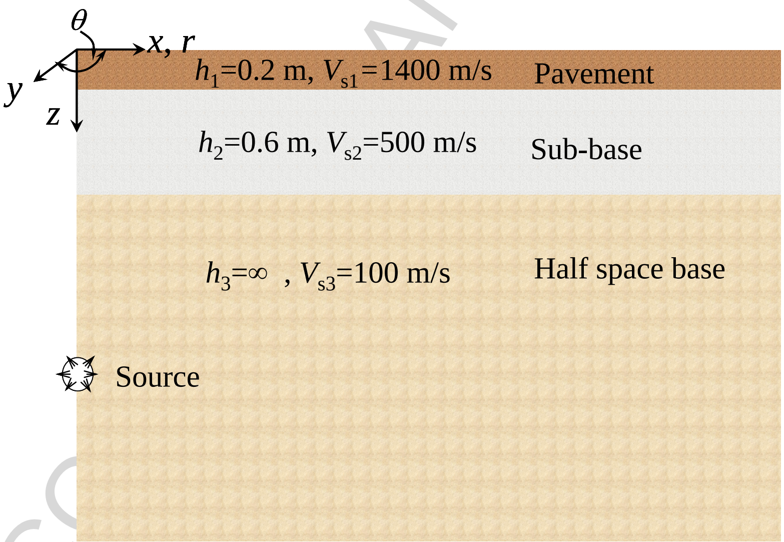

(b)

Fig. 1 Illustration of layer media, source and coordinate system: (a) layered half space; and (b) pavement.

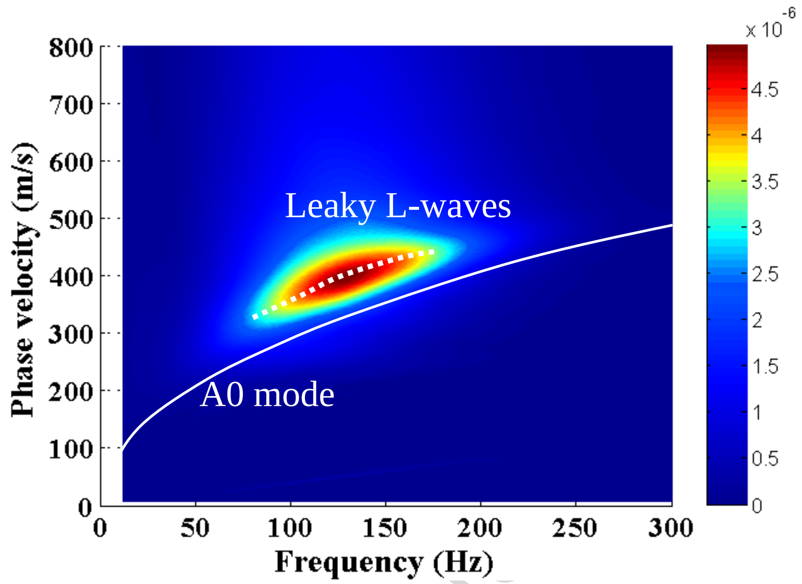

Fig. 2. Comparison of velocities of A0 mode and the leaky L-waves.

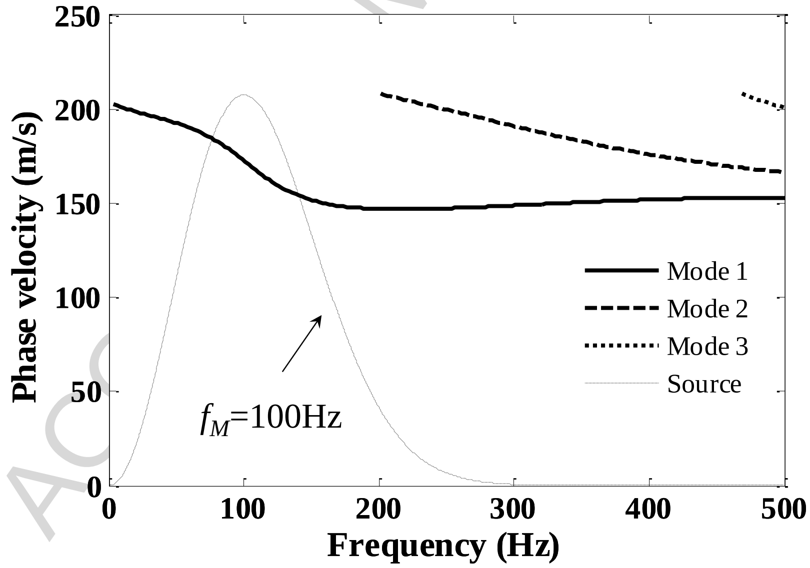

(a)

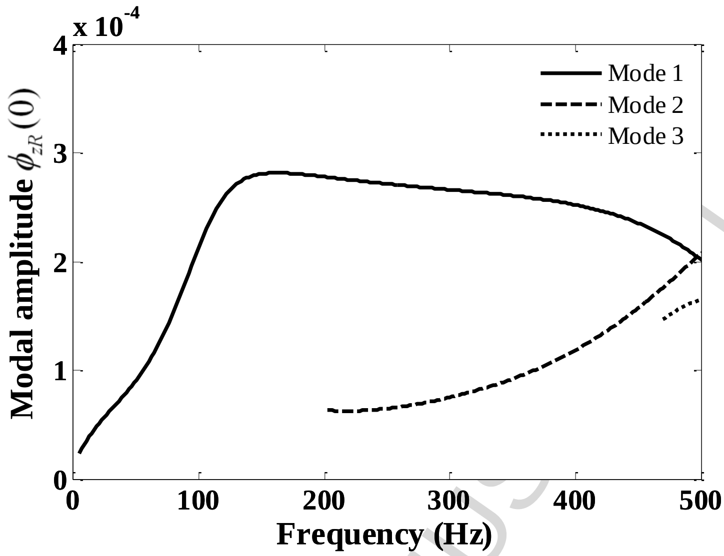

(b)

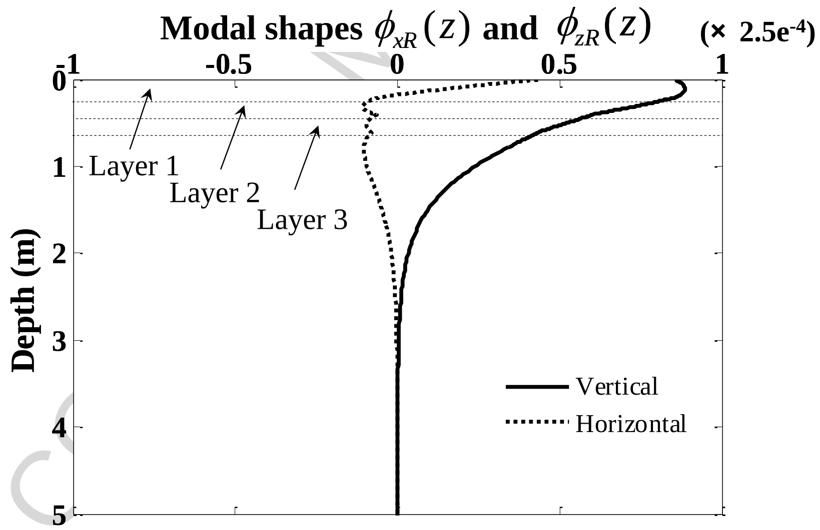

(c)

Fig. 3. Behavior of the normal R-wave modes in Case I: (a) dispersions; (b) surface modal amplitude $\phi_{zR}(0)$; and (c) horizontal and vertical modal shapes $\phi_{xR}(z)$ and $\phi_{zR}(z)$ at frequency of 100Hz.

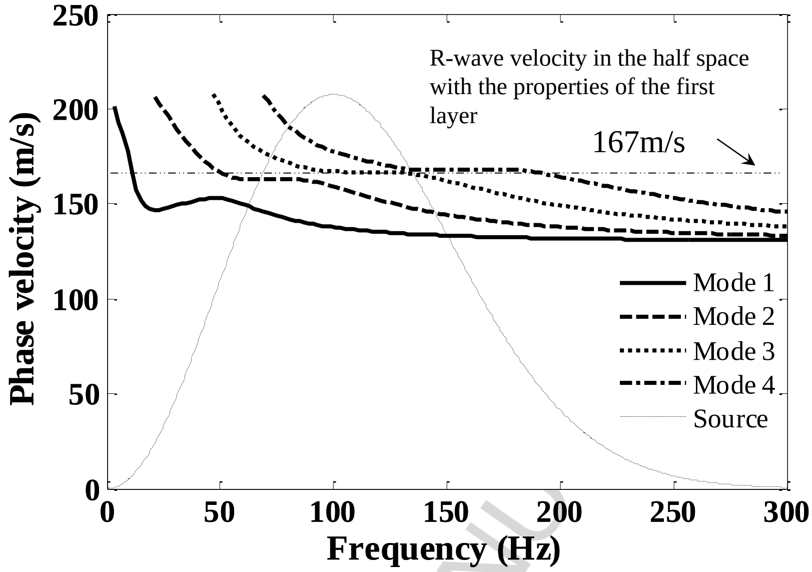

Phase velocity (m/s)
Frequency (Hz)
R-wave velocity in the half space with the properties of the first layer
167m/s
Mode 1
Mode 2
Mode 3
Mode 4
Source

(a)

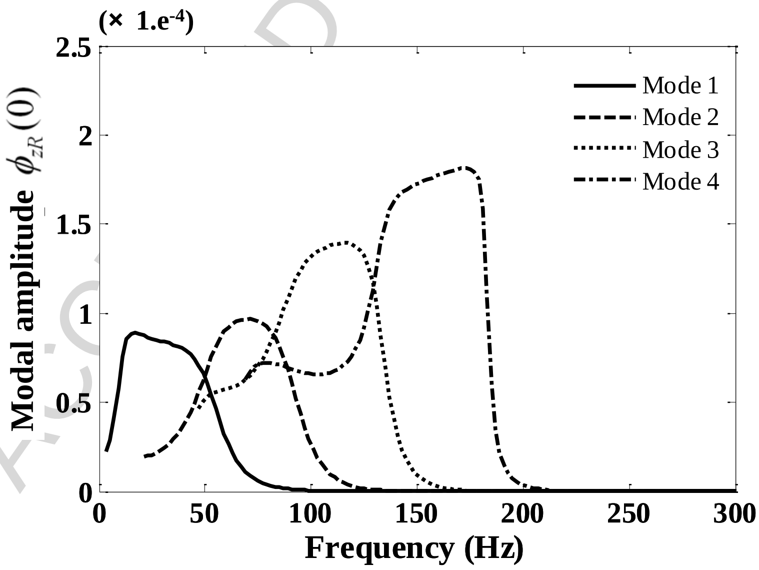

(× 1.e-4)
Modal amplitude $\phi_{zR}(0)$
Frequency (Hz)
Mode 1
Mode 2
Mode 3
Mode 4

(b)

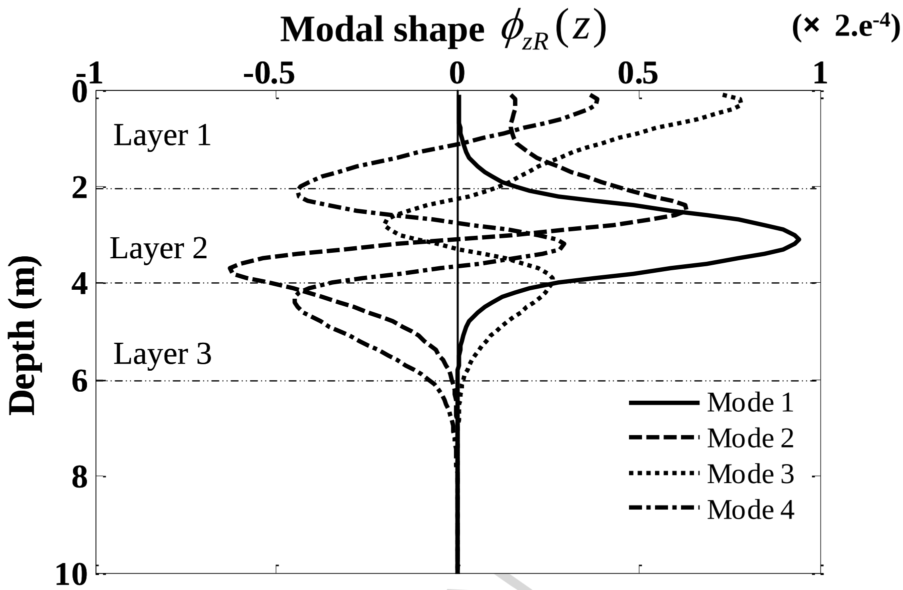

(c)

Fig. 4. Behavior of the first four normal modes of R-waves in Case II: (a) dispersions; (b) surface modal amplitude $\phi_{zR}(0)$; and (c) vertical modal shape $\phi_{zR}(z)$ at frequency of 100Hz.

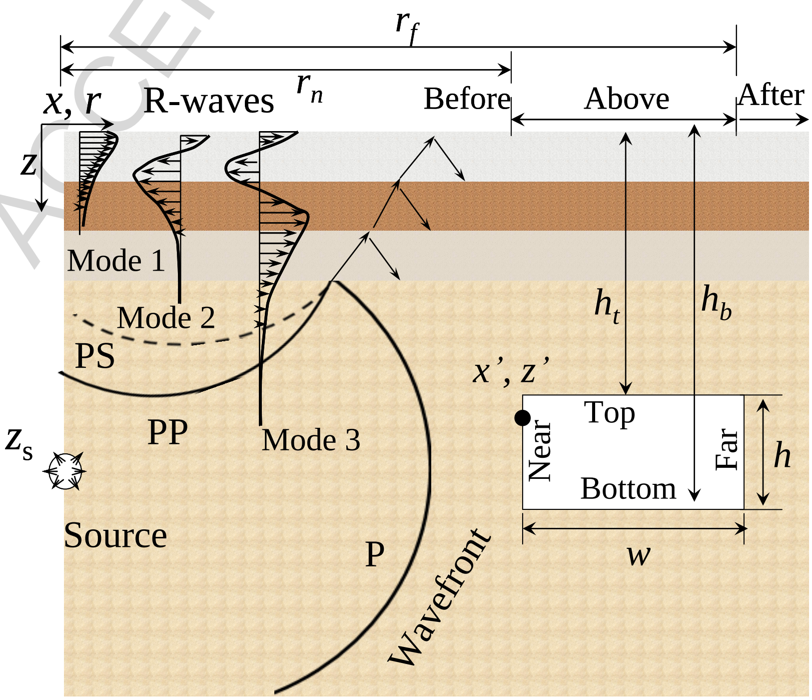

Fig. 5. Illustration of the wave types activated by a buried source and description of a

rectangular cavity.

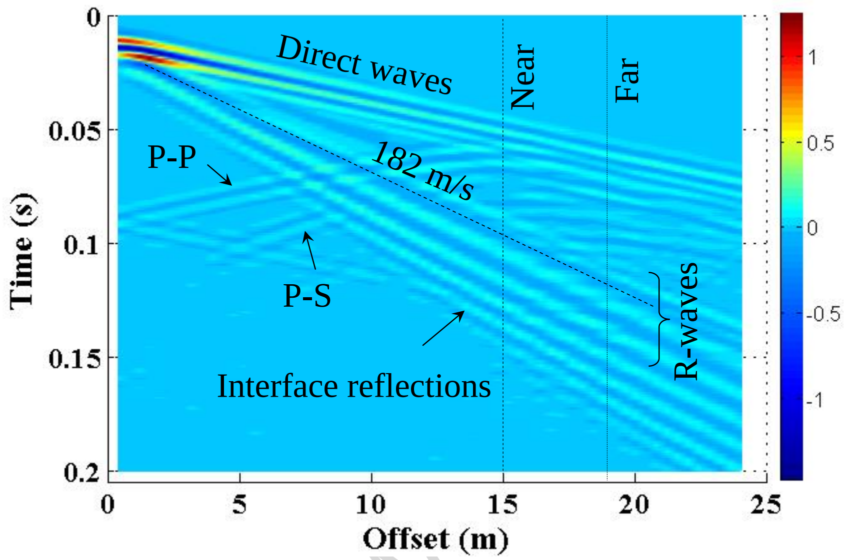

(a)

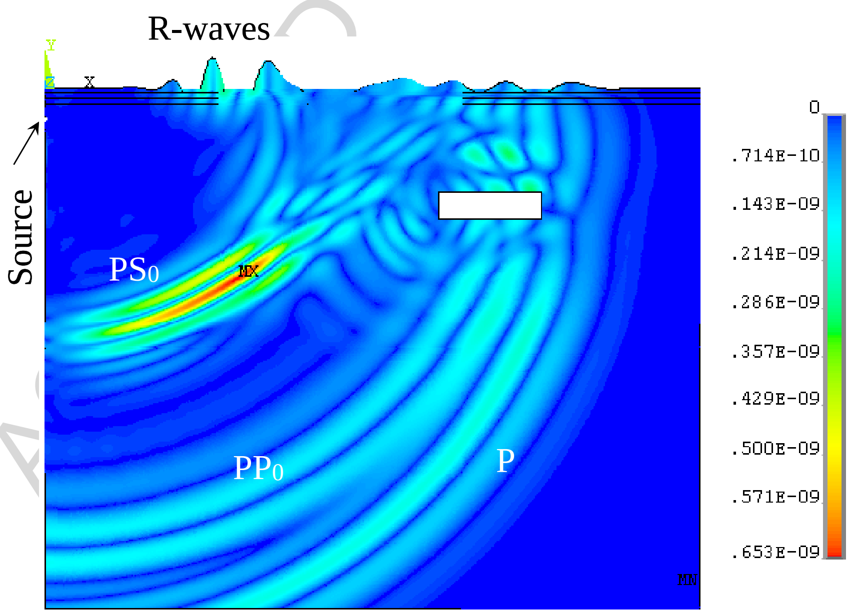

(b)

Fig. 6. Wave-field in Case I for the source at depth of 1.2 m: (a) contour plot of the surface responses; and (b) snapshot of particle velocity field.

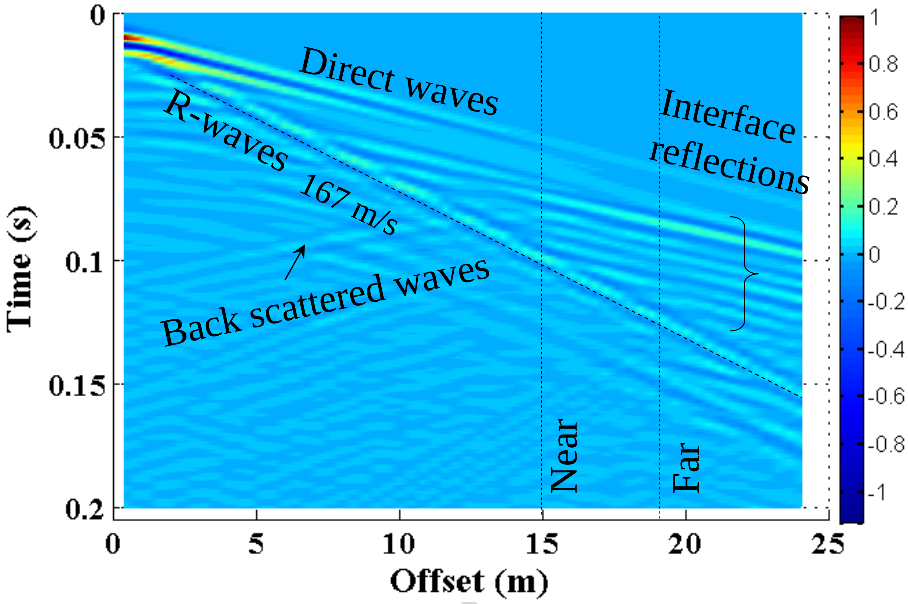

(a)

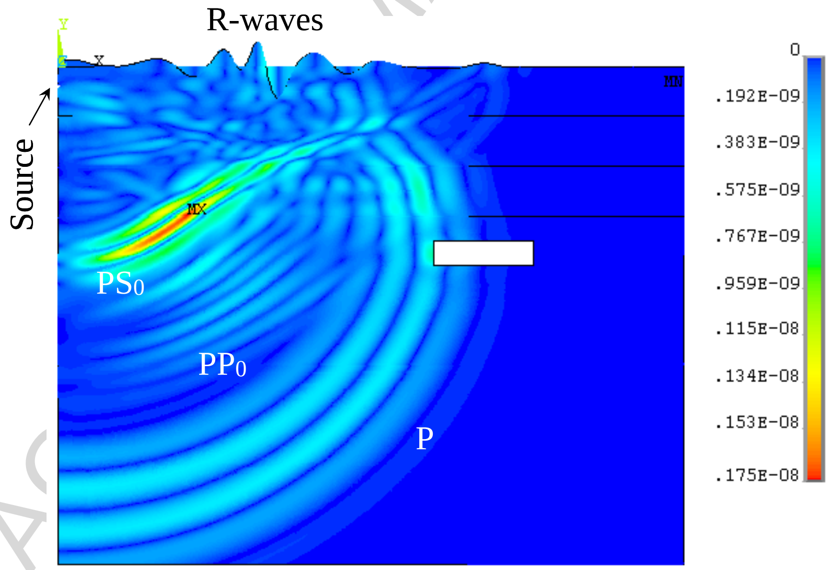

(b)

Fig. 7. Wave-field in Case II for the source at depth of 0.8 m: (a) contour plot of the surface responses; and (b) snapshot of particle velocity field.

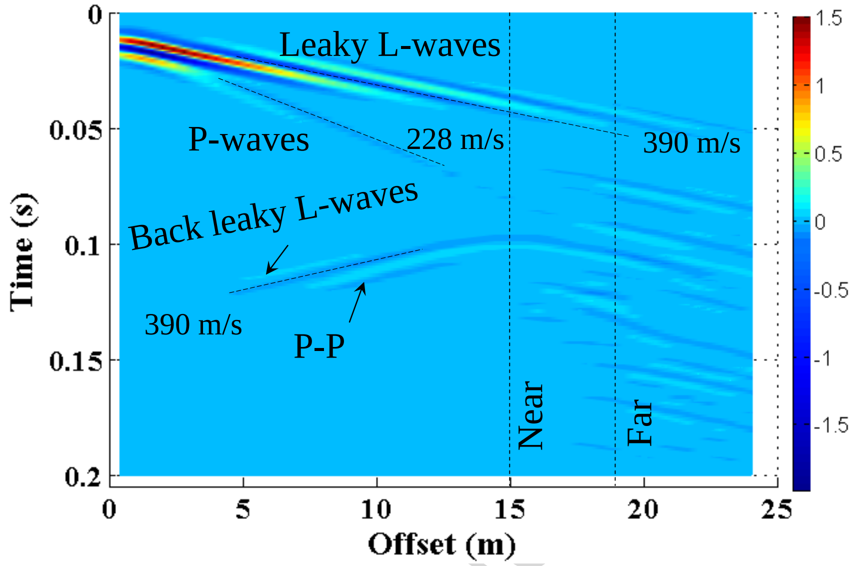

Fig. 8. Contour plot of the surface responses of the pavement system for the source at depth of 1.5 m.

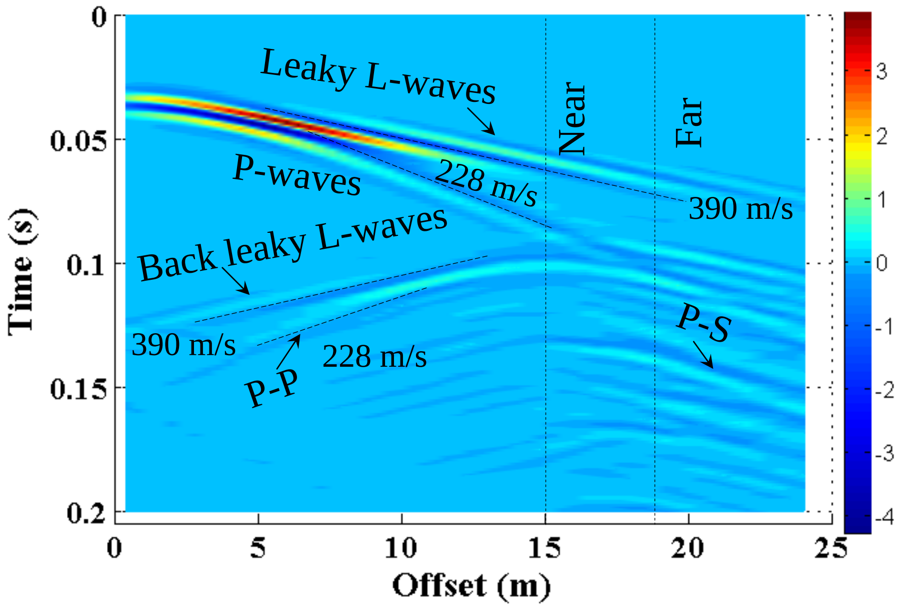

(a)

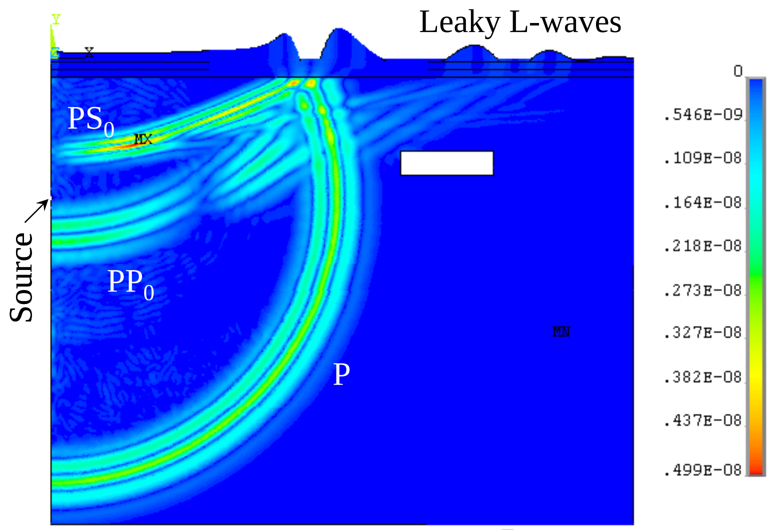

(b)

Fig. 9. Wave-field in the pavement system for the source at depth of 6 m: (a) contour plot of the surface responses; and (b) snapshot of particle velocity field.

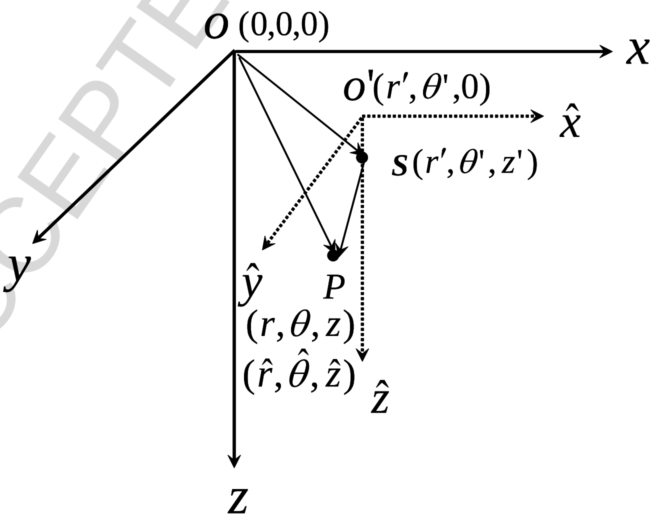

Fig. 10. Global and local coordinate systems (S: scattering point; P: observation point).

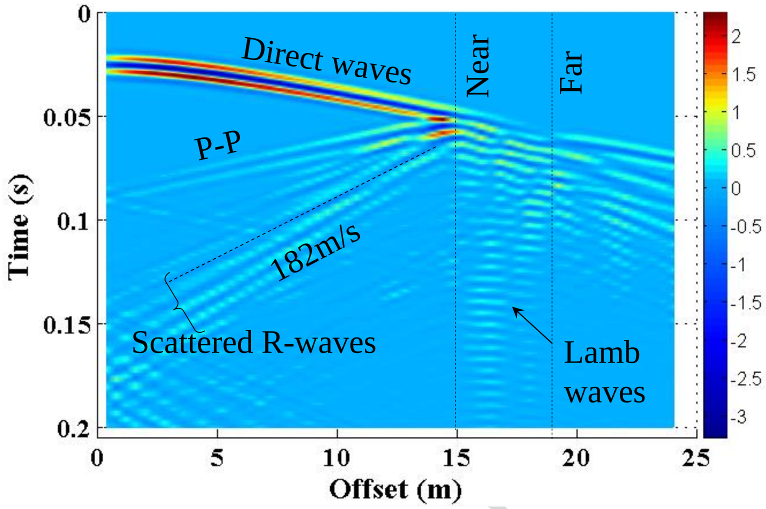

Fig. 11. Contour plot of the surface responses of Case I for the source at depth of 6 m and the rectangular cavity at r_n=15 m, r_f=19 m, h_t= 0.8 m and h_b=1.8 m.

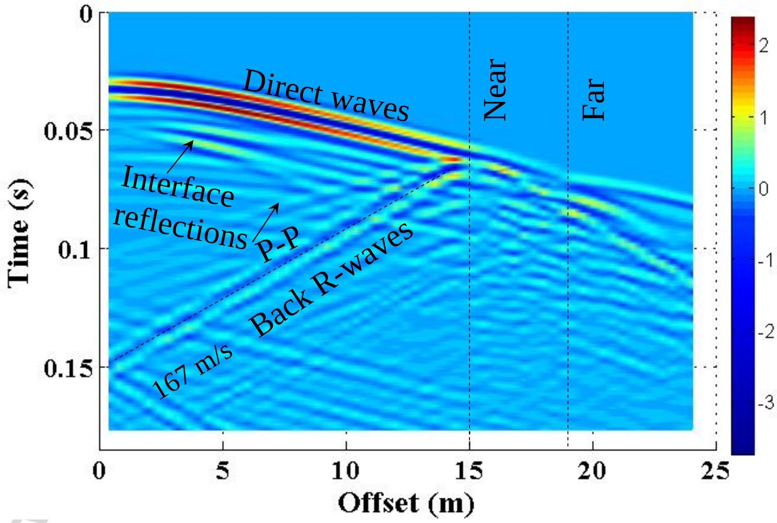

Fig. 12. Contour plot of the surface responses of Case II for the source at depth of 7 m and the rectangular cavity at r_n=15 m, r_f=19 m, h_t= 0.8 m and h_b=1.8 m.

568 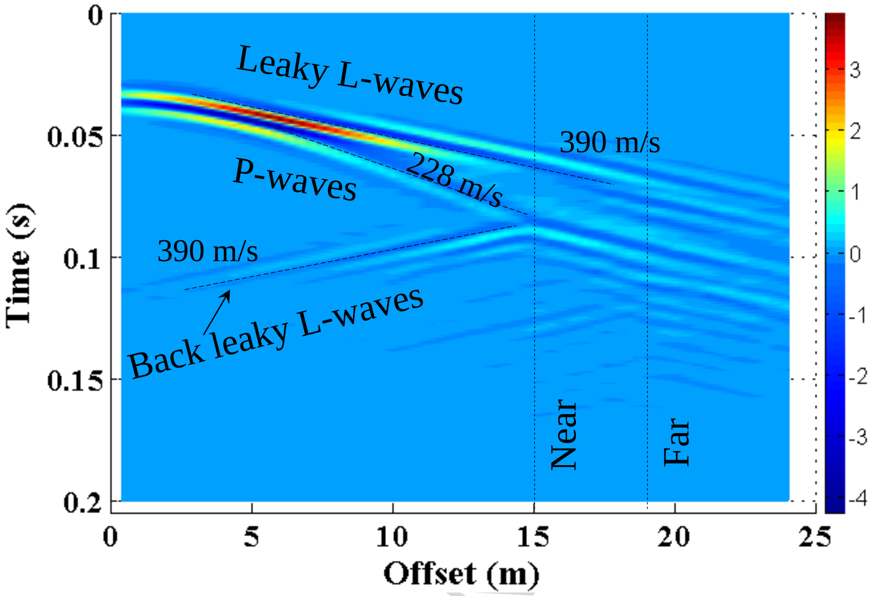

569 Fig. 13. Contour plot of the surface responses of the pavement system for the source

570 at depth of 6 m and the rectangular cavity at r_n=15 m, r_f=19 m, h_t= 1 m and h_b=2 m.